Check for updates

ChemistrySelect

ChemistrySelect
Chemistry Europe
European Chemical Societies Publishing

RESEARCH ARTICLE

Preparation and Characterization of Boron Nitride Coatings on Carbon Fibers From Functionalized Polyaminoboranes

Mert Burak Sen[1] | Müge Sarı Yılmaz[2] | Barış Yağcı[3] | Burcu Durçak[4] | Fadime Karaer Özmen[5,6] | Mustafa E. Üreyen[5,6] | Tarık Eren[1]

[1]Department of Chemistry, Yıldız Technical University, Esenler, Istanbul, Türkiye | [2]Department of Chemical Engineering, Yıldız Technical University, Esenler, Istanbul, Türkiye | [3]Koç University Surface Science and Technology Center (KUYTAM), Koç University, Sariyer, Istanbul, Türkiye | [4]Resin Chemist, DowAksa, Yalova, Türkiye | [5]Department of Fashion and Textile Design, Faculty of Architecture and Design, Eskisehir Technical University, Eskisehir, Turkey | [6]Advanced Technologies, Research Centre (ITAM), Eskisehir Technical University, Eskisehir, Turkey

Correspondence: Tarık Eren (teren@yildiz.edu.tr)

Received: 6 November 2025 | **Revised:** 17 November 2025 | **Accepted:** 28 November 2025

Keywords: boron nitride | carbon fibers | coatings | inorganic polymers | polyaminoborane synthesis

ABSTRACT

Polyaminoboranes, as inorganic analog of polyolefins, can be used to synthesize organic–inorganic hybrid ceramics, known as ceramers, and are typical examples of inorganic polymers. Here, p block elements, such as boron (B), silicon (Si), and phosphorus (P) possessing polyaminoborane homopolymers, were synthesized and characterized. After the synthesis of phosphorus–borane and amino silicon–borane complexes, polyaminoborane derivatives were obtained dehydrocoupling reaction in the presence of Grubbs catalyst. Boron nitride–phosphorus (P–BN) and boron nitride–silicon (Si–BN)-based ceramics were obtained under pyrolysis condition using polyaminoborane precursors. To demonstrate surface coating application, carbon fiber surface was dip-coated with polyaminoborane derivatives and pyrolyzed to get the functional boron nitride coating on the carbon fiber surface.

1 | Introduction

With an annual growth rate of 5%–6%, polyolefins, $[RCH\text{-}CH_2]_n$, are currently one of the most significant synthetic materials in the polymer industry [1]. Polyaminoboranes are inorganic analogs of polyolefins. The history of chemistry has been greatly influenced by the isoelectronic interaction between B–N and C–C bonds [2]. Applications for polyaminoboranes include the production of boron nitride (BN), dihydrogen storage, hydrogen cells, and energetic materials. Additionally, polyaminoboranes can serve as an example of a polymer with flame-retardant features due to the synergistic action of B and N. However, despite efforts made in the 1950s and 1960s, it was not possible to synthesize a soluble polyaminoborane $[RNH\text{-}BH_2]_n$ with high molecular weight and suitable characterization [3]. The catalytic dehydrogenation of primary amine–boranes and ammonia–boranes has offered a potential pathway for the production of analog of polyaminoboranes. Using $[Rh(\mu\text{-}Cl)(1,5\text{-}cod)]_2$ as a catalyst, a catalytic dehydrocoupling/dehydrogenation reaction was conducted with one equivalent of the complex to produce high molecular weight polyphosphinoboranes [4]. However, the desired product could not be achieved. Instead, formation of weakly insoluble and branched oligomeric materials was observed [5]. $NH_3{\cdot}BH_3$, a cyclic pentamer followed by $[NH_2BH_2]_5$, was synthesized using Brookhart's IrH_2POCOP catalyst. This development has facilitated similar studies in the preparation of soluble polyaminoboranes with primary amine–borane additives [6]. Similar to the previously described catalytic dehydroconjugation/dehydrogenation of primary phosphine borane adducts, the catalytic dehydrogenation of primary amine–boranes and

This article is dedicated to emeritus Prof. Dr. Evamarie Hey-Hawkins.

© 2025 Wiley-VCH GmbH

ammonia-boranes offers a possible pathway to polyaminoboranes. Staubitz et al. demonstrated the success of polyaminoborane synthesis by conducting Rh-catalyzed dehydroconjugation of primary amine–borane adducts [2]. They achieved this synthesis by utilizing an amine–borane adduct such as $CH_3NH_2{:}BH_3$ at ambient temperature in the presence of a catalyst. This approach led to the identification of well-characterized, high molecular weight, and soluble polyaminoboranes, and it was achieved through the room temperature reaction of $MeNH_2{\cdot}BH_3$, one of the readily available amine–borane additive precursors [2–7]. As an alternative, dehydrogenation of an amine–borane was also studied to make an extremely reactive aminoborane, followed by the subsequent dehydrogenation of this reactive aminoborane to produce polyaminoborane polymers [8–11]. Recently, a well-defined polymer, *N*-methyl polyaminoborane $(H_2BNMeH)_n$, was obtained at a high yield using an air-tolerant catalyst system [11]. Previously, Hey-Hawkins et al. synthesized phosphorus–boron-based polymers obtained by dehydrocoupling of ferrocenylphosphine–borane adducts using $[Rh(\mu\text{-}Cl)(cod)_2]$ (cod = 1,5-cyclooctadiene) catalyst [12]. High thermal stability was achieved for all polymers, and 40–80 wt% char yield was obtained at 1000°C. Polyaminoborane synthesis can also be performed without using a catalyst. Alcaraz et al. successfully synthesized polyaminoborane polymers without the use of a catalyst, providing an alternative approach [13, 14]. Diisopropylaminoborane (iPr_2NBH_2; DIAB) served as the monomer precursor in the procedure outlined. The in situ produced monomer, in contrast to the sterically hindered iPr_2NBH_2, is thermally unstable and polymerizes right away. This method of synthetic synthesis produces polymers with extremely high molecular weights without the use of solvents or metal catalysts.

Polyaminoboranes are precursors for boron nitride (BN). BN is a layered material with high thermal and chemical stability, which is ideal for coating applications with remarkable thermal conductivity [15]. Hexagonal and cubic boron nitride (isoelectronically comparable to graphite and diamond) have been used in various industries [16, 17], including aerospace [18], automotive [19], electronics [20], semiconductors [21, 22], and cosmetics industries [23]. In its cubic form (c-BN), it is the second hardest material after diamond, showcasing remarkable resistance to flames and corrosion. Hexagonal boron nitride (h-BN), resembling graphite, possesses a wide range of features, including strong electrical resistance, minimal thermal expansion, resistance to thermal shock, high thermal conductivity, non-toxicity, ease of machining, lubricity, chemical inertness, and resistance to wetting by several molten metals [24, 25]. h-BN is a wide-bandgap semiconductor (6 eV) with potential uses in UV lasing and as a dielectric material, in contrast to a single layer of graphite (graphene) that has a band gap of zero [26]. Depending on its structure, boron nitride exhibits unique characteristics as a non-oxide ceramic material. Polyaminoboranes and polyborazylenes have shown promise as an alternative for boron nitride production among preceramic polymers. Figure 1 shows the structure of polyborazylenes and polyaminoborane. The synthesis of polyborazylene generally involves the cyclotetramerization of diborane and ammonia or other nitrogen sources. The cyclotetramerization process leads to the formation of borazane rings, which eventually polymerize to form the polyborazylene chain. Polyborazylene synthesis is sensitive to oxygen and moisture, which can disrupt the reaction and lead

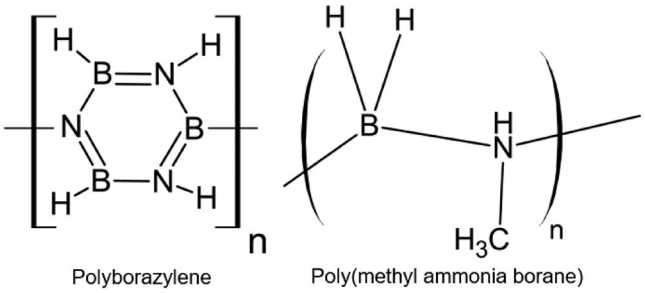


FIGURE 1 | Structure of polyborazylenes and polymethylaminoborane.

to undesired by-products. Apart from the inert atmosphere and catalyst, other reaction conditions, such as temperature, pressure, and reaction time, can also affect the yield and properties of polyborazylene. Optimizing these parameters is essential to achieve the desired results [27]. However, polyaminoboranes can dissolve in common solvents and are easily processable onto common materials using dip coating, spraying, and spin-coating processes. The polymer structure transforms into a boron nitride ceramic after pyrolysis (>1000°C). Therefore, that can be an advantage when used regularly in coating applications and simple macromolecular processing [28]. A variety of possible uses for polyaminoboranes as a high-performance ceramic are of interest [29]. Methyl-polyaminoboranes were pyrolyzed to produce amorphous nanostructures with an h-BN component [29]. The pyrolysis of polyaminoboranes and methyl-polyaminoboranes produces polydisperse, amorphous B, and N-containing spherical nanoparticles from H_3NBH_3, which can be seen on rhodium foil as a substrate. The advantage of preceramic polyaminoboranes lies in their potential for machinability, allowing for the fabrication of BN coating on complex-shaped materials [29–31]. It is possible to achieve a uniform deposition of boron nitride onto the surface [32].

The addition of phosphorous and silicon to boron nitride from polyaminoborane could enhance the composites' thermal conductivity to some extent. Boron-nitride products with silica and phosphorous may increase the density of residual char in case of its flame retardancy and thermal stability [33]. Phosphate coating has been widely used in the surface treatments of vehicles and steel buildings due to good adherence and lubricity [34]. Silicon's increased barrier property may be used to substantially increase the corrosion resistance of the coating [35]. The addition of silicon to boron nitride can result in boron nitrides with improved thermal conductivity and lubricity [36]. The oxyphilic nature of the phosphorus makes the materials absorb oxygen groups [37, 38]. This increases the oxidative stability in harsh conditions. Thus, phosphor and silicon-based boron nitride ceramics can show multifunctional properties. In this study, methyl-based polyaminoboranes, phosphorous-based polyaminoboranes, and silicon-based polyaminoboranes were synthesized. Homopolymers of these functional polyaminoboranes were used to synthesize methylene-containing boron nitride (CH_3-BN), phosphorous-containing boron nitride (P-BN), and silicon-containing boron nitride (Si-BN) after pyrolysis. The characterization of the monomers and polymers at each stage led to the discovery of the intended structures as products. To demonstrate the surface application of these products, the carbon fiber

23656549, 2025, 47, Downloaded from https://chemistry-europe.onlinelibrary.wiley.com/doi/10.1002/slct.202506905 by Yildiz Teknik University, Wiley Online Library on [16/12/2025]. See the Terms and Conditions (https://onlinelibrary.wiley.com/terms-and-conditions) on Wiley Online Library for rules of use; OA articles are governed by the applicable Creative Commons License

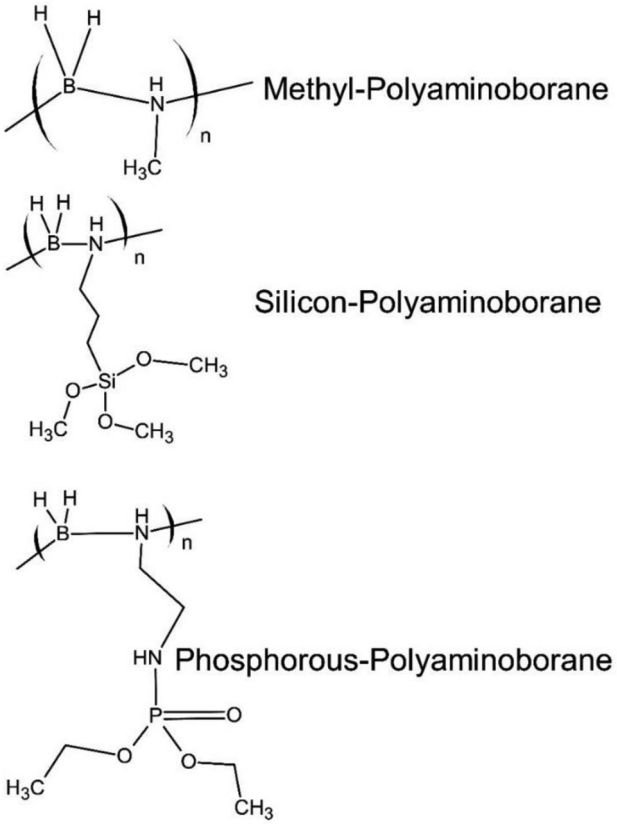


FIGURE 2 | Structure of polyaminoborane homopolymers synthesized in this study.

surface was coated with the dip coating method. X-ray photoelectron spectroscopy (XPS), nuclear magnetic resonance (NMR), Fourier transform infrared spectroscopy (FT-IR), scanning electron microscopy energy–dispersive x-ray spectroscopy (SEM–EDX), and thermogravimetric analysis (TGA) analyses were conducted to study the characteristics of the polyaminoborane precursors and functional boron nitride. Figure 2 shows the functional polyaminoboranes synthesized in this study.

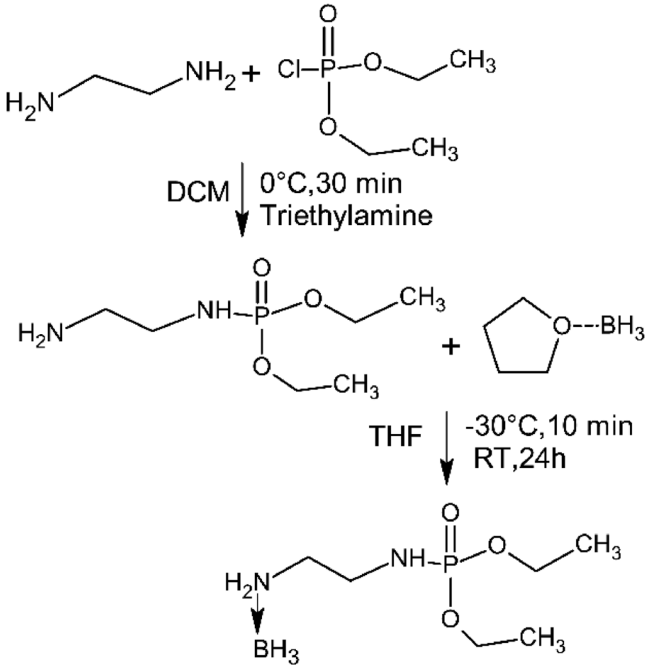
2 | Results and Discussion

2.1 | Synthesis and Characterization of Homopolymers

2.1.1 | Methyl-Substituted Polyaminoborane

Methyl-substituted polyaminoboranes were synthesized according to the literature [2], with the use of a modified catalyst system. *N*-methylamine–borane served as the monomer, where the methyl substituent was intended to act as a solubilizing side chain. First, methyl-substituted polyaminoborane was synthesized using the catalyst 1,3-bis(2,4,6-trimethylphenyl)-2-imidazolidinylidene)-dichloro(phenylmethylene)(tricyclohexylphosphine)ruthenium. After the work-up, yellow–brown solid residue was obtained at a yield of 40%. Synthetic scheme can be observed in Scheme S1.

The obtained polymer was characterized by FT-IR, NMR, TGA, gel permeation chromatography (GPC), and XPS analyses. In the



SCHEME 1 | Synthesis of phosphorus-based amino borane precursor.

^{11}B NMR spectrum (Figure S1), a resonance appeared at −7.9 ppm, confirming the formation of a methyl-substituted amino borane environment. This value is notably less negative than the typical B–N–H region (−15 to −20 ppm), suggesting an altered electronic environment around boron. The upfield shift is attributed to the electron-donating effect of the methyl substituent and possible local coordination or cross-linking interactions within the polymer backbone.

The FT-IR spectrum (Figure S2) displayed a broad N–H stretching band at ~3240 cm^{-1}, C–H stretching from methyl groups near 2960 cm^{-1}, and a distinct B–H stretching mode at 2274 cm^{-1}. The N–H bending appeared around 1600 cm^{-1}, whereas C–H bending vibrations were observed near 1320 cm^{-1}. A characteristic B–N stretching vibration was detected at ~1160 cm^{-1}, confirming the formation of the B–N backbone.

GPC analysis in dimethylformamide (DMF) containing 8 wt% LiCl calibrated with polystyrene standards revealed a moderate polydispersity ($Đ = 1.3$) and a number-average molecular weight (M_n) of 4.9×10^3 g mol^{-1} (Table S1, Figure S3).

2.1.2 | Phosphorous-Substituted Polyaminoboranes

A phosphorus-based amino borane precursor (Scheme 1) was synthesized as the initial step toward preparing the phosphorus-substituted polyaminoborane. For this purpose, ethylenediamine was reacted with diethyl chlorophosphate in the presence of trimethylamine as a base in dichloromethane. After work-up, a white precipitate was isolated in 33% yield. The structure of the precursor, diethyl (2-aminoethyl)phosphoramidate was confirmed by ^{1}H and ^{13}C NMR spectroscopy (Figures S4 and S5).

In the ^{1}H NMR spectrum ($CDCl_3$), a broad singlet at around 8 ppm corresponds to the secondary amine (–NH–) proton bound to

23656549, 2025, 47, Downloaded from https://chemistry-europe.onlinelibrary.wiley.com/doi/10.1002/slct.202506905 by Yildiz Teknik University, Wiley Online Library on [16/12/2025]. See the Terms and Conditions (https://onlinelibrary.wiley.com/terms-and-conditions) on Wiley Online Library for rules of use; OA articles are governed by the applicable Creative Commons License

phosphorus. Its pronounced broadness and downfield position are consistent with hydrogen bonding and possible coupling to ^{31}P. The O–CH_2– protons of the diethyl phosphonate ester appear as multiplets at 4.0–4.3 ppm, characteristic of methylene groups attached to oxygen in a phosphoryl environment. A broad signal centered around 5.0 ppm is assigned to the –NH_2 protons. The NH_2 protons are not distinctly visible, likely due to proton exchange and broadening through solvent and temperature effects, which is typical for primary amines. Multiplets near 2.0 ppm correspond to CH_2 groups adjacent to the terminal –NH_2, whereas additional resonances around 1.6 ppm are attributed to internal CH_2 groups (NH–CH_2–CH_2–NH_2), slightly deshielded by neighboring phosphorus and nitrogen atoms. The ethyl methyl (–CH_3) groups of the diethyl ester are observed as triplets at 1.2–1.4 and 0.9–1.1 ppm, suggesting two slightly different local electronic environments for the two ethoxy substituents.

The ^{13}C NMR spectrum ($CDCl_3$) showed a prominent signal at 60 ppm, corresponding to the C–O–P(=O) carbon, confirming the phosphonate linkage. The –CH_2–NH_2 carbon of the ethylenediamine chain appeared at 29 ppm, whereas the methyl carbons (–CH_3) of the diethyl groups resonated between 10 and 15 ppm, consistent with terminal alkyl carbons attached through oxygen. The slightly upfield position relative to typical aliphatic methyl carbons (~15–20 ppm) can be attributed to the shielding effect of the P–O bond.

Phosphorus-based amino borane precursor was synthesized using borane–tetrahydrofuran complexes. For structural characterization, the FT-IR spectra of the phosphorus-substituted amino borane precursor (Figures S6 and S7) showed a broad N–H stretching band centered at ≈3180 cm^{-1}, characteristic of amine groups. A pair of B–H stretching absorptions appeared only in Figure S7, at 2360 and 2260 cm^{-1}, confirming borane coordination [2]. Strong bands at 1230 and 960 cm^{-1} correspond to P═O stretching and P–O vibration, respectively [39]. Additional C–H stretching at ≈2900 cm^{-1} and bending vibrations at 1465 cm^{-1} arise from ethyl substituents. Relative to the methyl-substituted polyaminoborane, the N–H stretching band appears at a slightly lower frequency (3180 vs. 3240 cm^{-1}), owing to the electron-withdrawing phosphoryl group and stronger hydrogen-bonding interactions in the P–N–BH_3 framework. The ^{31}P NMR spectrum ($CDCl_3$, Figure S8) exhibited a single resonance at δ = 9.05 ppm, consistent with a tetra-coordinated phosphonate environment and the complete substitution of P–Cl bonds [40]. In the ^{1}H NMR spectrum ($CDCl_3$, Figure S9), signals at 4.0–4.3 ppm correspond to the O–CH_2 protons of the diethyl ester. The BH_3-coordinated NH_2 protons, expected between 3.5 and 4.0 ppm, are not distinctly visible, most likely because they overlap with the O–CH_2 quartet and appear as a weak, broadened shoulder. Such overlap and line broadening are typical for BH_3–amine complexes, where rapid proton exchange and coupling with boron cause diffuse, unresolved features. A triplet at 1.3 ppm corresponds to the methyl (–CH_3) protons of the ethoxy groups, and a very broad, low-intensity band between 0.5 and 1.5 ppm is attributable to hydridic B–H protons. The secondary amine (–NH–) proton, theoretically expected around 7.8–8.0 ppm, is not observed, which is common for such species due to strong hydrogen bonding and partial overlap with the solvent residual signal ($CDCl_3$ at 7.26 ppm).

The ^{13}C NMR spectrum ($CDCl_3$, Figure S10) displayed resonances at ≈61 ppm (O–CH_2), 41.7 ppm (BH_3-coordinated NH_2–CH_2), 28.7 ppm (NH–CH_2–P), and ≈15 ppm (CH_3). The carbon chemical shifts are consistent with literature values for amine–borane phosphonate systems, confirming the expected connectivity and the electron-withdrawing influence of the P═O group.

The ^{11}B NMR spectrum (Figure S11) showed a broad resonance at δ = −9.40 ppm, characteristic of a BH_3–NH_2 coordination complex. This value lies within the typical range (−10 to −25 ppm) for amine–borane adducts and confirms the formation of a stable B–N dative bond in the phosphorus-substituted precursor [41]. Collectively, these spectral data confirm the successful synthesis of the BH_3-stabilized phosphorus-based amino borane precursor, distinguished by its diagnostic B–H stretching doublet (2360/2260 cm^{-1}), P═O (1230 cm^{-1}) and P–O (960 cm^{-1}) vibrations, and the ^{11}B NMR resonance at −9.4 ppm indicative of intact B–N coordination.

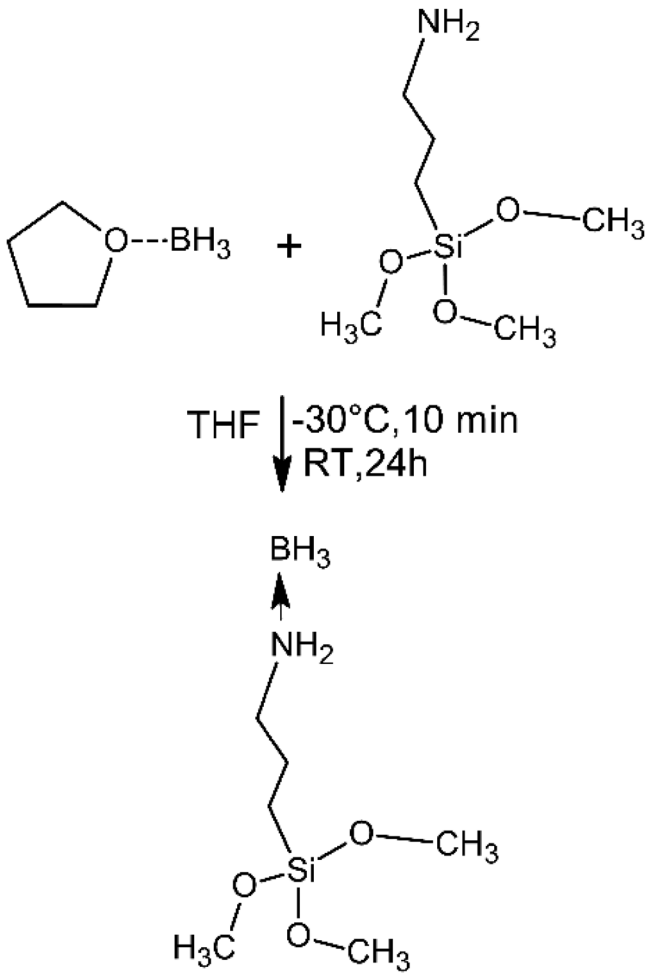
The phosphorus-substituted amino borane precursor was polymerized to obtain a phosphorus-based polyaminoborane, designed to achieve a boron–phosphorus–nitrogen synergistic effect within the polymer backbone (Scheme S2). The phosphorus-substituted precursor was dissolved in tetrahydrofuran(THF) to obtain a 10-M solution and treated with 0.1 mol% of the catalyst 1,3-bis(2,4,6-trimethylphenyl)-2-imidazolidinylidene)-dichloro(phenylmethylene)(tricyclohexylphosphine)ruthenium at 0°C. As a result of this reaction, light brown coloration in the reaction mixture was observed. After the work-up of the polymer, the light brown precipitate was obtained at a yield of 50%. TGA, GPC, and XPS were also carried out in addition to FT-IR and NMR for the characterization of the polymer. In the ^{11}B NMR spectrum (Figure S13), a broad resonance centered at δ = −7.03 ppm was observed, typical of a four-coordinate B–N environment in polymeric amino boranes. The single-broad peak reflects a uniform boron coordination environment throughout the chain and the absence of unreacted borane species. The FT-IR spectrum of the phosphorus-substituted polyaminoborane (Figure S12) exhibited diagnostic absorptions at 3270 cm^{-1} (N–H stretching), 2370 cm^{-1} (B–H stretching), and ≈2900 cm^{-1} (aliphatic C–H stretching). A clear C–H bending band was observed at 1414 cm^{-1}. Strong absorptions at 1250 cm^{-1} (P═O stretching) and 960 cm^{-1} (P–O vibration) confirmed the retention of the phosphoramidate side group. Additional bands between 1020 and 950 cm^{-1} were assigned to overlapping B–N and C–N stretching modes characteristic of the polyaminoborane backbone. These features collectively verify that both the B–N polymeric framework and the P–O–C functional substituents remain intact after polymerization The ^{31}P NMR spectrum (Figure S14) displayed a single sharp signal at δ = 17.57 ppm, consistent with a phosphoryl nitrogen-bonded (P═O)$(OEt)_2$–NH– moiety. The chemical shift matches reported values for phosphoramidate-type phosphorus centers, confirming that the P–N bond remained intact during polymerization [42]. Molecular-weight analysis by GPC (8% LiCl/DMF as eluent, calibrated with polystyrene standards) revealed a number-average molecular weight (M_n) of 4.8 × 10^4 g mol^{-1} and a polydispersity index ($Đ$) of 1.3 (Table S1 and Figure S3).

23656549, 2025, 47, Downloaded from https://chemistry-europe.onlinelibrary.wiley.com/doi/10.1002/slct.202506905 by Yildiz Teknik University, Wiley Online Library on [16/12/2025]. See the Terms and Conditions (https://onlinelibrary.wiley.com/terms-and-conditions) on Wiley Online Library for rules of use; OA articles are governed by the applicable Creative Commons License

2.1.3 | Silicon-Substituted Polyaminoborane

First, silicon-substituted precursor was synthesized to produce the targeted functional polyaminoborane. Thus, 3-aminopropyltrimethoxysilane in THF was reacted with BH_3:THF complex, and a white viscous residue was observed after 2 h. This residue was washed with cold diethyl ether and pentane mixture. The yield of the white precipitate precursor was found to be 25% (Scheme 2).

The silicon-containing amino borane precursor was synthesized by coordinating borane–tetrahydrofuran with a trimethoxysilane-linked amine, forming a BH_3–amine adduct. Structural characterization was carried out by FT-IR and NMR spectroscopy. In the FT-IR spectrum (Figure S15), a pair of absorptions at 2305–2377 cm^{-1} confirmed the presence of B–H stretching vibrations characteristic of amino borane complexes. A broad N–H stretching band appeared at ≈3150 cm^{-1}, whereas B–N stretching was observed at 1329 cm^{-1}. Aliphatic C–H stretching was detected near 2900 cm^{-1}, and Si–O–C stretching appeared at 1033 cm^{-1}, both consistent with a trimethoxysilyl environment [43]. The ^1H NMR spectrum ($CDCl_3$, Figure S16) showed a singlet at 3.5 ppm for methoxy protons (Si–OCH_3), a triplet at 2.7 ppm assigned to CH_2 groups adjacent to the NH_2–BH_3 unit, and a multiplet between 1.3 and 1.7 ppm corresponding to internal CH_2 groups in the alkyl chain. A triplet at 0.65 ppm was attributed to Si–CH_2– protons. A broad quartet between 0.9 and 1.3 ppm was assigned to BH_3 hydrides. Weak, broad signals between 4.0 and 5.0 ppm correspond to NH_2 protons bound to boron, which are not distinctly visible due to proton exchange and hydrogen-bond broadening, typical for primary amine–borane adducts. The ^{11}B NMR spectrum (Figure S17) displayed a single resonance at $\delta = -19.63$ ppm, consistent with a four-coordinate BH_3–NH_2 complex, confirming complete formation of the amine–borane adduct. The ^{29}Si NMR (Figure S18) exhibited a broad signal centered at $\delta \approx -70$ ppm, characteristic of a Q^4-type $Si(OSi)_4$ siloxane network, suggesting partial hydrolysis and condensation of methoxysilane groups during work-up. After the work-up of silicon-substituted polyaminoborane, a white solid precipitate was obtained at a yield of 65%. For the polymer characterization, FT-IR, NMR, TGA, GPC, and XPS were performed. The FT-IR spectrum of the silicon-based polyaminoborane (Figure S19) showed broad absorptions at ≈3200 cm^{-1} (N–H stretching), 2300–2350 cm^{-1} (B–H stretching), 2900 cm^{-1} (C–H stretching), 1329 cm^{-1} (B–N stretching), and 1040 cm^{-1} (Si–O–C stretching). These bands verify the coexistence of amino borane and siloxane functionalities, indicating formation of a B–N–Si hybrid polymer network. The ^{11}B NMR and ^{29}Si NMR analyses in Figures S20 and S21 show the presence of boron and silicon bonds in the polymer structure. The ^{11}B spectra show the expected broad signals at −7.0 ppm. Silicone derived structure was observed in ^{29}Si NMR around −120 ppm. The ^{11}B NMR spectrum (Figure S20) exhibited a broad resonance centered at $\delta = -24.80$ ppm, consistent with four-coordinate boron centers within the polymeric B–N backbone. The ^{29}Si NMR spectrum (Figure S21) displayed a broad peak around $\delta \approx -128$ ppm, confirming the persistence of a siloxane-derived environment after polymerization, indicative of extended Si–O–Si condensation. Silicon-based polyaminoborane in GPC analysis resulted in a molecular weight of 3.9×10^4 g mol^{-1} with a $Đ$ value of 1.9 (see Table S1 and Figure S3).



SCHEME 2 | Synthesis of silicon-based amino borane precursor.

2.2 | Thermal Analysis of the Functional Polyaminoboranes

TGA analyses of homopolymers were performed under air and nitrogen atmospheres (Table S2, Figures 3 and 4). Polyaminoborane derivatives showed high thermal stability even at 800°C. Under a nitrogen atmosphere, the silicon functional polyaminoboranes had the highest char yield (60%) at 800°C. However, the char yields of the phosphorous and methyl functional polyaminoboranes series at 800°C were found to be 45% and 42%, respectively. The high char yield of the silicon functional polyaminoborane can be explained by the silicon bond being relatively stable under thermal treatment. The cleavage of phosphorous-ester bonds most likely increases the degradation profile of phosphorus-bearing polyaminoboranes compared to the silicon based polyaminoborane. The energy required to break silicon-carbon bonds is typically higher, leading to their greater stability under thermal conditions. Phosphorus-ester bonds are inherently more susceptible to cleavage under thermal stress compared to silicon–oxygen bonds.

Under the air atmosphere, different thermal behaviors were observed. Methyl-polyaminoboranes series had the highest char yield (58%) at 800°C. However, silicon and phosphorous pos-

23656549, 2025, 47, Downloaded from https://chemistry-europe.onlinelibrary.wiley.com/doi/10.1002/slct.202506905 by Yildiz Teknik University, Wiley Online Library on [16/12/2025]. See the Terms and Conditions (https://onlinelibrary.wiley.com/terms-and-conditions) on Wiley Online Library for rules of use; OA articles are governed by the applicable Creative Commons License

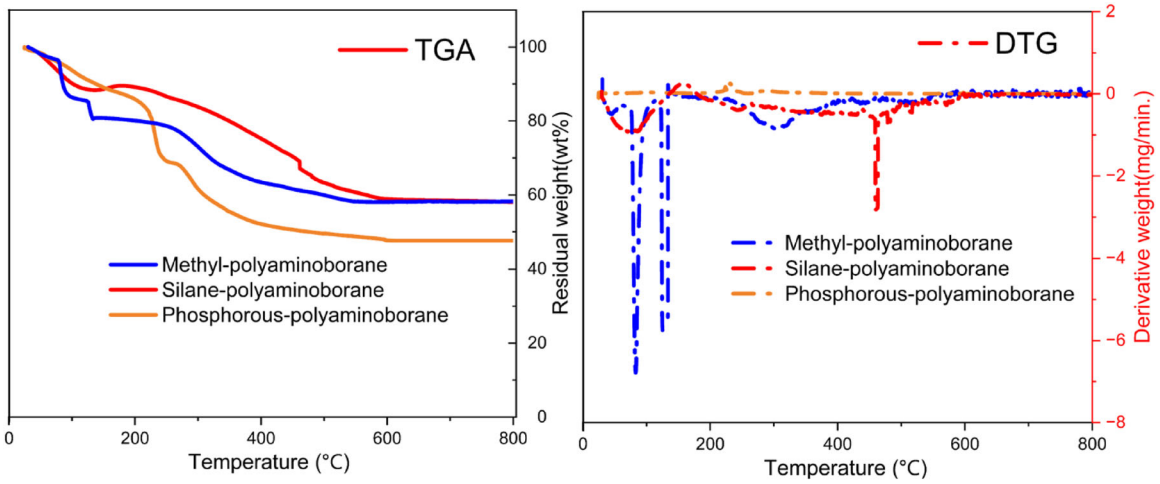


FIGURE 3 | TGA–DTG curve representing thermal decomposition of polyaminoboranes under air atmosphere. DTG, derivative thermogravimetric; TGA, thermogravimetric analysis.

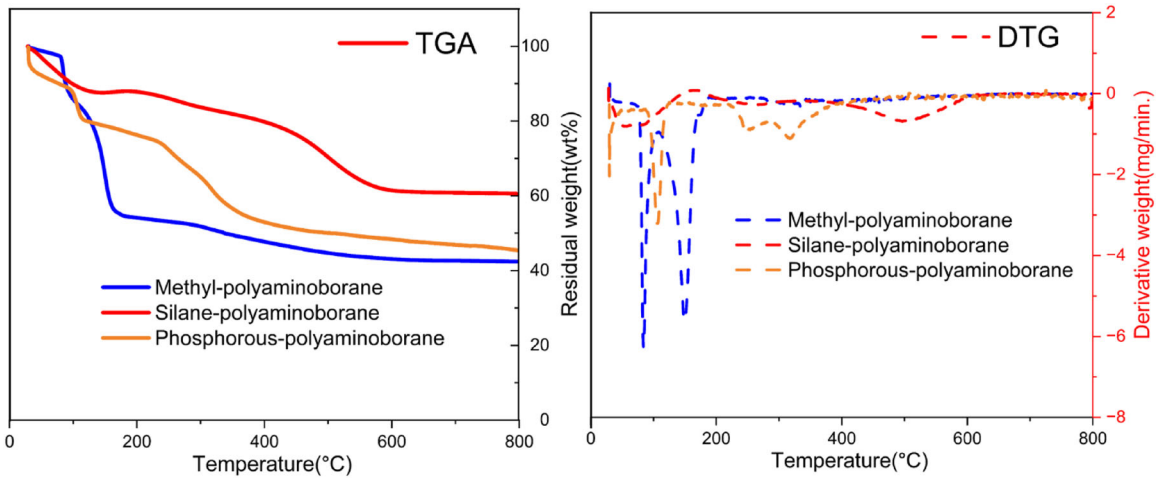


FIGURE 4 | TGA–DTG curve representing thermal decomposition of polyaminoboranes under nitrogen atmosphere. DTG, derivative thermogravimetric; TGA, thermogravimetric analysis.

sessing polyaminoboranes series led to 45% and 47% char yield, respectively. These relatively lower char yields compared to methyl-based polyaminoboranes can be due to the cleavage of silicon and phosphorous functional groups under oxygen. Table S3 summarizes the char yield of each homopolymer series under air and nitrogen atmosphere.

The derivative thermogravimetric (DTG) profiles of the polyaminoborane series under nitrogen and oxygen atmospheres reveal distinct thermal degradation mechanisms and stability patterns. Under the nitrogen atmosphere, all polyaminoboranes display two main decomposition stages corresponding to polymer backbone scission and subsequent rearrangement into boron nitride–rich ceramic residues. The absence of oxygen limits oxidation reactions, resulting in purely pyrolytic decomposition with moderate char formation. Among the series, the methyl-polyaminoborane exhibits two well-defined DTG peaks, indicating sequential loss of volatile species and formation of a thermally stable BN framework. In contrast, under the oxygen atmosphere, the DTG curves exhibit multiple overlapping events, reflecting complex oxidation–ceramization behavior. At lower temperatures (around 200°C for methyl and phosphorus-containing samples, and 220°C for the silane derivative), a transient mass gain is observed, attributed to oxygen uptake and the formation of protective oxide or borate layers (such as SiO_2 and B_2O_3). Subsequent DTG peaks correspond to exothermic oxidation of organic fragments, leading to the densification of inorganic residues. Overall, the DTG analysis confirms that the presence of heteroatom substituents modulates both the onset and rate of decomposition: Nitrogen favors controlled pyrolysis, whereas oxygen promotes concurrent oxidation and oxide formation. The protective glassy layers (SiO_2, B_2O_3) formed during oxidation contribute to enhanced char yields and improved thermal stability, particularly for the methyl-based system.

Microscale combustion calorimetry (MCC) analysis was also applied to acquire the flammability of borane polymer. MCC has been successively used for flammability characteristics, such as the total heat release (THR), heat release capacity (HRC), peak heat release rate (PHRR), and temperature at peak heat release of materials. As a result of MCC analysis, the values of the

23656549, 2025, 47, Downloaded from https://chemistry-europe.onlinelibrary.wiley.com/doi/10.1002/slct.202506905 by Yildiz Teknik University, Wiley Online Library on [16/12/2025]. See the Terms and Conditions (https://onlinelibrary.wiley.com/terms-and-conditions) on Wiley Online Library for rules of use; OA articles are governed by the applicable Creative Commons License

average HRC, PHRR, THR, and temperature at PHRR (TPHRR) can be obtained for all polymers. The HRR or the PHRR are major parameters in determining for the analysis of fire risk of materials. For example, the lower the HRR value shows the higher the incombustibility of the polymer. We observed that the PHRR values of polymers phosphorus-polyaminoborane, methyl-polyaminoborane, and silicon-polyaminoborane homopolymers are 442, 102, and 33 W g^{-1}, respectively (Figure 5). The introduction of a phosphate ester group into the polymer could result in a dramatic change in the decomposition process; however, silane containing polyaminoborane displays the highest non-flammability properties. This can be attributed to the phosphonate group cleavage from the matrix during the thermal treatment. This profile indicates rapid devolatilization once degradation begins and limited char retention—that is, a larger fraction of mass converts to combustible volatiles in a narrow temperature window. Silicon–polyaminoborane (red) exhibits a delayed, broader, and much lower HRR peak at higher temperature, consistent with suppressed volatilization and enhanced condensed-phase stabilization (silica/siloxane-like residue acting as a barrier). Methyl-polyaminoborane (blue) has a small early peak that quickly decays to near-baseline, suggesting limited THR and/or the formation of a stabilized char/ceramic-like residue that throttles further fuel release. To sum up, Si–polyaminoborane shows the most favorable fire-performance signature (low, delayed HRR), methyl-polyaminoborane looks promising via early passivation, and phosphorus-polyaminoborane appears most prone to rapid fuel release under these conditions—useful guidance for selecting or modifying backbones toward micro-/cone performance.

2.3 | XPS Analysis of the Functional Polyaminoboranes

XPS analysis of the homopolymer series was performed to investigate the chemical composition and bonding states of the polymers (Figure 6). The spectra confirmed that heteroatom substitution at the boron–nitrogen backbone induces distinct electronic changes in the local environment of B and N atoms. For the methyl-substituted polyaminoborane, the binding energies of N1s, B1s, C1s, and O1s are observed at approximately 400, 189, 285, and 530 eV, respectively. The B1s region displays two components at 189 eV (B–N) and 192 eV (B–O), corresponding to the boron–nitrogen backbone and minor surface oxidation, respectively. The N1s spectrum shows a main peak at 400 eV, attributed to N–H or B–N bonding, and a shoulder near 398 eV, assigned to sp^2-hybridized nitrogen in BN-like environments. The C1s peak around 285 eV corresponds to C–H, C–O, and C–N groups from methyl substituents, whereas the O1s signal near 530 eV arises from adsorbed oxygen species on the surface [44]. Overall, these results confirm the formation of a polyaminoborane backbone consisting of B–N–H repeat units, with minor oxidation due to ambient exposure.

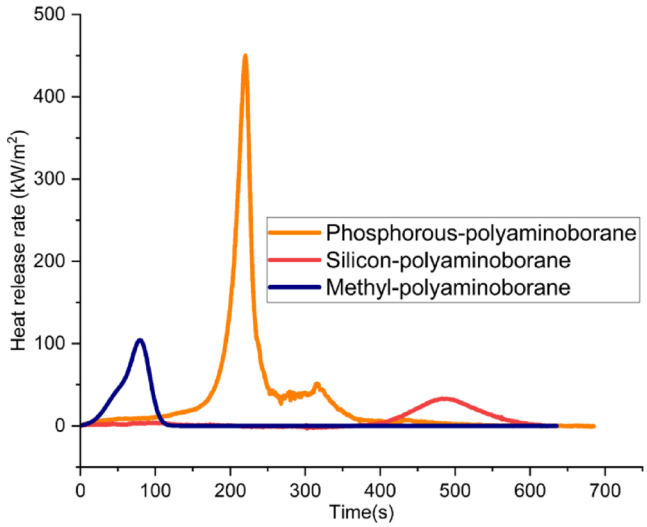


FIGURE 5 | Microscale combustion calorimetry for polyaminoborane homopolymers.

For the phosphorus-substituted polyaminoborane, XPS spectra of C1s, O1s, N1s, P2p, and B1s reveal the coexistence of boron–nitrogen, boron–phosphorus, and phosphorus–oxygen environments. The C1s region shows three main components centered at ~285 eV (C–H/C–C), ~286 eV (C–O–P), and ~288 eV (C═O), the latter attributed to carbonyl groups associated with amide or phosphonate moieties. The O1s peak near 530 eV is consistent with phosphoryl and B–O bonds. The P2p signal appears at 133–134 eV, corresponding to P–N/P–B and P–O bonds, confirming the presence of a phosphonate-like structure within the polymer matrix [45]. The N1s peaks at ~399–401 eV can be assigned to B–N, N–P, and partially oxidized N–O environments, whereas the B1s spectrum exhibits three components at 189 eV (B–N), 191 eV (B–N–P or B–O–P), and 192 eV (oxidized B–O). These findings demonstrate that phosphorus substitution induces a positive shift in the B1s binding energy, indicating a more electron-withdrawing environment for boron and the successful incorporation of P–N and P–B linkages into the polymer backbone. In the silicon-substituted polyaminoborane, the XPS results show similar chemical trends but with distinct silicon-related features. The Si2p peaks at 102 eV (Si–N/Si–C) and 103 eV (Si–O) confirm the coexistence of silazane (Si–N–B) and oxidized SiO species. The B1s peak centered at 192 eV indicates partial oxidation (B–O–Si) and electron deficiency around boron due to the inductive effect of silicon. The N1s components at 398–401 eV correspond to B–N, N–Si, and oxidized nitrogen sites, verifying the formation of Si–N–B linkages in the polymer structure.

In summary, XPS results confirm that all polymer derivatives preserve the B–N framework characteristic of polyaminoborane, whereas substitution with Si or P introduces B–N–Si and B–N–P linkages. These chemical modifications not only alter the electron density around boron and nitrogen but also enhance the potential of the polymers as precursors for BN-based ceramics with tunable compositions upon pyrolysis under inert conditions.

2.4 | Synthesis and Characterization of Functional Boron Nitride Ceramics

Polyaminoboranes are typical precursors for the synthesis of boron-nitride ceramic materials. In this study, phosphorus (P–BN), silicon (Si–BN) functional BN structures were synthesized using respective functional polyaminoboranes. These materials are expected to have variety of uses, including surface coating,

23656549, 2025, 47, Downloaded from https://chemistry-europe.onlinelibrary.wiley.com/doi/10.1002/slct.202506905 by Yildiz Teknik Universitesi, Wiley Online Library on [16/12/2025]. See the Terms and Conditions (https://onlinelibrary.wiley.com/terms-and-conditions) on Wiley Online Library for rules of use; OA articles are governed by the applicable Creative Commons License

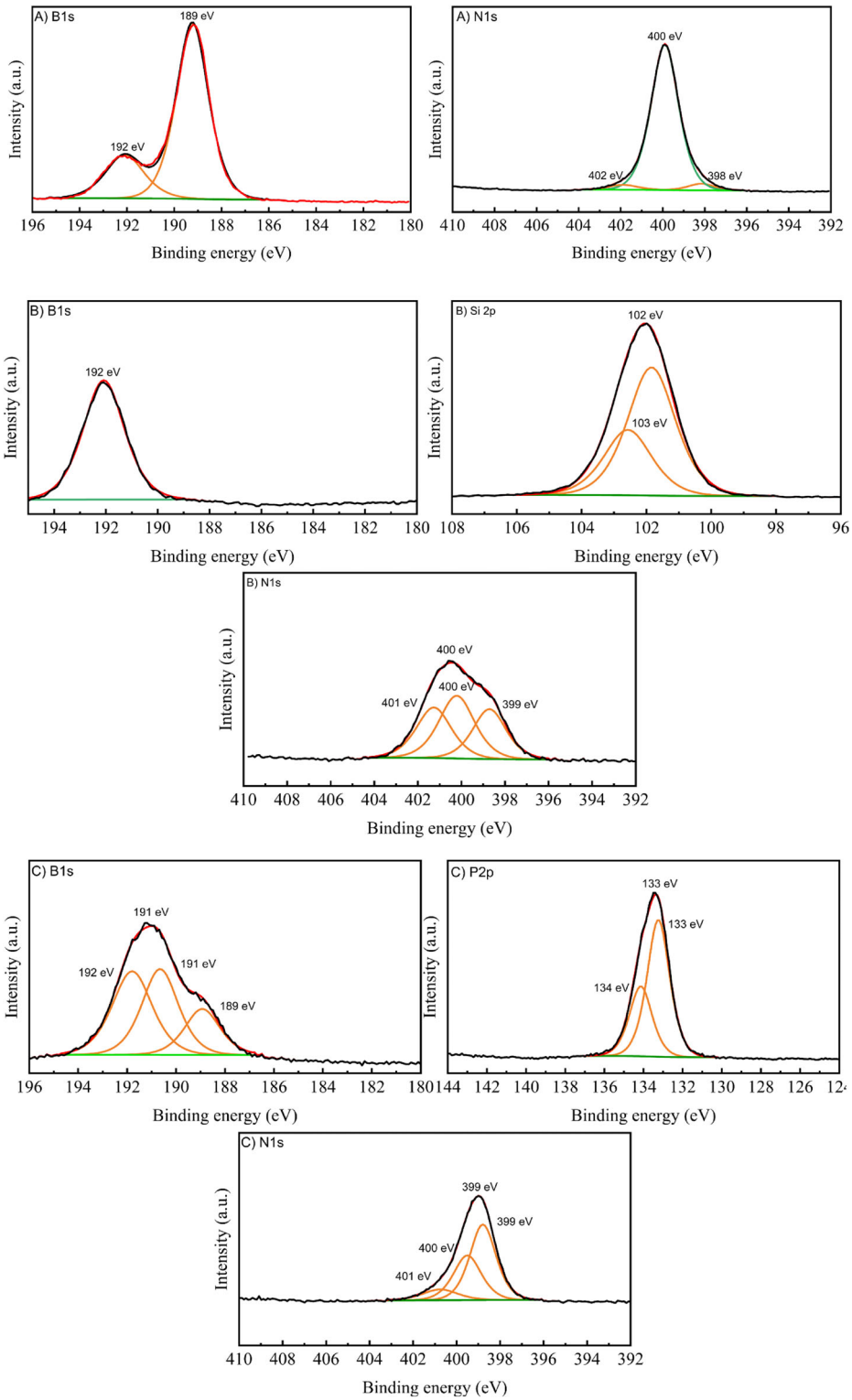


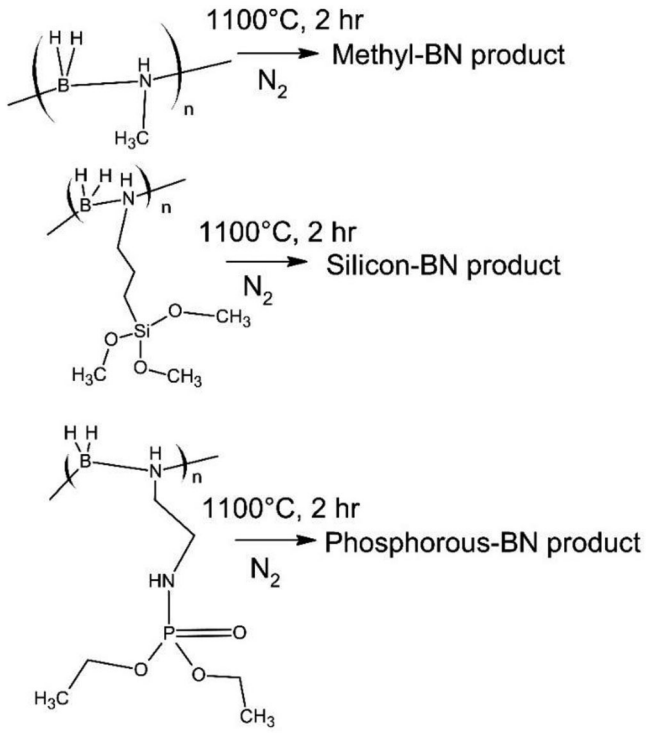
FIGURE 6 | XPS analysis for homopolymers of polyaminoborane: (A) methyl-substituted polyaminoborane, (B) silicon-substituted polyaminoborane, and (C) phosphorus-substituted polyaminoborane.

where they may be used to create a surface that is strong, durable, and extremely wear-resistant.

For the production of boron nitride, an atmosphere-controlled tube furnace system was used to perform pyrolysis, whereas nitrogen flowed through the tube at a rate of 2 L min^{-1}. Pyrolysis of methyl, silicon, and phosphorus bearing polyaminoboranes homopolymer series were carried out under nitrogen for 2 h at 1100°C (Scheme 3).

In order to characterize boron nitride structures, first x-ray diffraction (XRD) analysis was used. The polymers and the orig-

23656549, 2025, 47, Downloaded from https://chemistry-europe.onlinelibrary.wiley.com/doi/10.1002/slct.202506905 by Yildiz Teknik University, Wiley Online Library on [16/12/2025]. See the Terms and Conditions (https://onlinelibrary.wiley.com/terms-and-conditions) on Wiley Online Library for rules of use; OA articles are governed by the applicable Creative Commons License



SCHEME 3 | Synthesis of boron nitride from homopolymer series.

inal bulk material (BN) underwent crystalline structure characterization using XRD in Figure S22. With a noticeable and clearly defined peak at $2\theta = 29°$ [44], the XRD patterns showed a highly crystalline structure as hexagonal boron nitride. Methyl, silicon, and phosphorous boron nitride ceramics showed the diffraction peaks for hexagonal boron nitride. For methyl-polyaminoborane, there is a peak around $2\theta = 40°$ [44], and this peak defines boron nitride. Silicon and phosphorous polyaminoboranes have amorphous B–H bond around $2\theta = 15°$ [46].

2.5 | Functional Boron Nitride Coating on Carbon Fiber

The BN coating provides several benefits to carbon fiber materials, such as improved thermal stability [47], electrical insulation [48], oxidation resistance [49], and friction reduction [50]. These specific properties and performance of a BN-coated carbon fiber can be based on deposition method, thickness, and functional groups present in crystal structures. The process of applying BN coating to carbon fiber typically involves chemical vapor deposition (CVD) [51] or physical vapor deposition (PVD) [52] techniques. Here, methyl and silicon functional polyaminoboranes series were used as precursors for the BN synthesis. Polymers were dissolved in THF 10% (w/v) and filament of carbon fiber was dipped into this solution for half an hour. Then, coated carbon fiber was removed from the solution and dried under vacuum. Boron nitride coating was formed by applying a thermal treatment at 1100°C for 2 h under nitrogen. Figure 7 shows the typical coating procedure.

Characterization of the carbon fiber surface and its ceramic coating was conducted using XPS, TGA, and SEM–EDX analyses. The XPS results (Figure 8) confirm the successful formation of boron nitride (BN) coatings derived from both methyl- and silicon-containing polyaminoborane precursors. After coating, a significant increase in nitrogen content was observed, which is consistent with the formation of a BN-type structure on the fiber surface. Bare carbon fibers contain more than 90% carbon [53]. Residual silicon is also present in the bare carbon fibers due to their production process. In the survey spectrum of the uncoated fiber, peaks at approximately 285 eV are attributed to C–H and C–C bonds, whereas the signal at 288 eV corresponds to carbonyl (C═O) groups that typically form during oxidation or surface treatment of the carbon fiber. Following the coating process, the emergence of characteristic boron and nitrogen peaks demonstrates the formation of BN species. The B1s spectra show two major components centered around 190–191 and 193 eV, assigned to B–N and B–O bonds, respectively. The N1s spectrum exhibits a primary peak near 399–400 eV, corresponding to B–N and N–C bonding environments, and a minor component at higher binding energy (~401 eV), attributed to oxidized or protonated nitrogen species.

For the BN coating derived from methyl-polyaminoborane, the XPS data are consistent with the formation of a largely stoichiometric BN network, with dominant B–N and N–B–N environments. The B1s spectrum of the methyl-derived BN exhibits a major component at ~190 eV (B–N) and a smaller one at ~192 eV (B–O), which can be attributed to mild surface oxidation after air exposure. The N1s spectrum shows a strong signal at ~398 eV, characteristic of sp^2-hybridized nitrogen in a hexagonal BN-like environment, and a weaker feature at ~400 eV corresponding to N–H or surface nitrogen. These results confirm that the pyrolysis of methyl-polyaminoborane yields a BN-type ceramic with a composition close to h-BN, while retaining some surface oxynitride character. In contrast, coatings derived from silicon-containing polyaminoborane precursors display distinct spectral features associated with the incorporation of silicon into the BN framework. In the B1s spectrum, the main B–N peak is slightly shifted to ~191 eV, indicating an altered electronic environment due to the presence of Si–N–B linkages. The higher energy component at ~193 eV becomes more pronounced, consistent with B–O–Si or B–O moieties formed by surface oxidation or interfacial Si–O–B bonding. The Si 2p spectrum exhibits peaks at ~103 and ~104 eV, assigned to Si–N and Si–O bonds, respectively, confirming that Si atoms are successfully integrated into the ceramic network. The predominant Si–N peak signifies that silicon participates primarily in nitridic coordination, whereas the Si–O feature likely arises from thin surface oxide formation upon exposure to air [45]. The N1s spectrum of the Si-modified BN shows two overlapping components at 399 and 401 eV. The lower-energy signal corresponds to nitrogen atoms bridging boron and silicon (B–N–Si environments), whereas the higher energy contribution originates from oxidized or protonated nitrogen species. The coexistence of these peaks suggests the formation of a mixed Si–B–N network, where Si–N bonding alters the local charge distribution of the BN framework. This structural modification is further reflected in the observed shifts of B1s binding energies and the increased intensity of oxygen-containing peaks, both indicative of enhanced crosslinking and partial surface oxidation at Si sites. Overall, these XPS findings demonstrate that both precursor systems undergo complete transformation into nitridic ceramic networks upon pyrolysis, yet the chemical environments and

23656549, 2025, 47, Downloaded from https://chemistry-europe.onlinelibrary.wiley.com/doi/10.1002/slct.202506905 by Yildiz Teknik University, Wiley Online Library on [16/12/2025]. See the Terms and Conditions (https://onlinelibrary.wiley.com/terms-and-conditions) on Wiley Online Library for rules of use; OA articles are governed by the applicable Creative Commons License

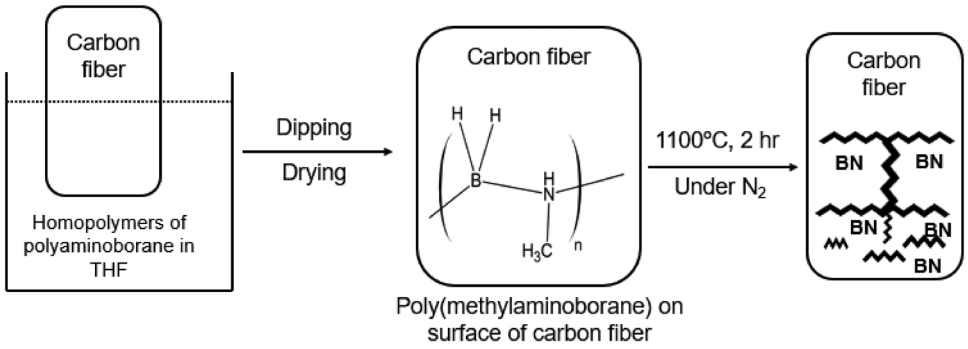


FIGURE 7 | Boron nitride coating process for carbon fiber.

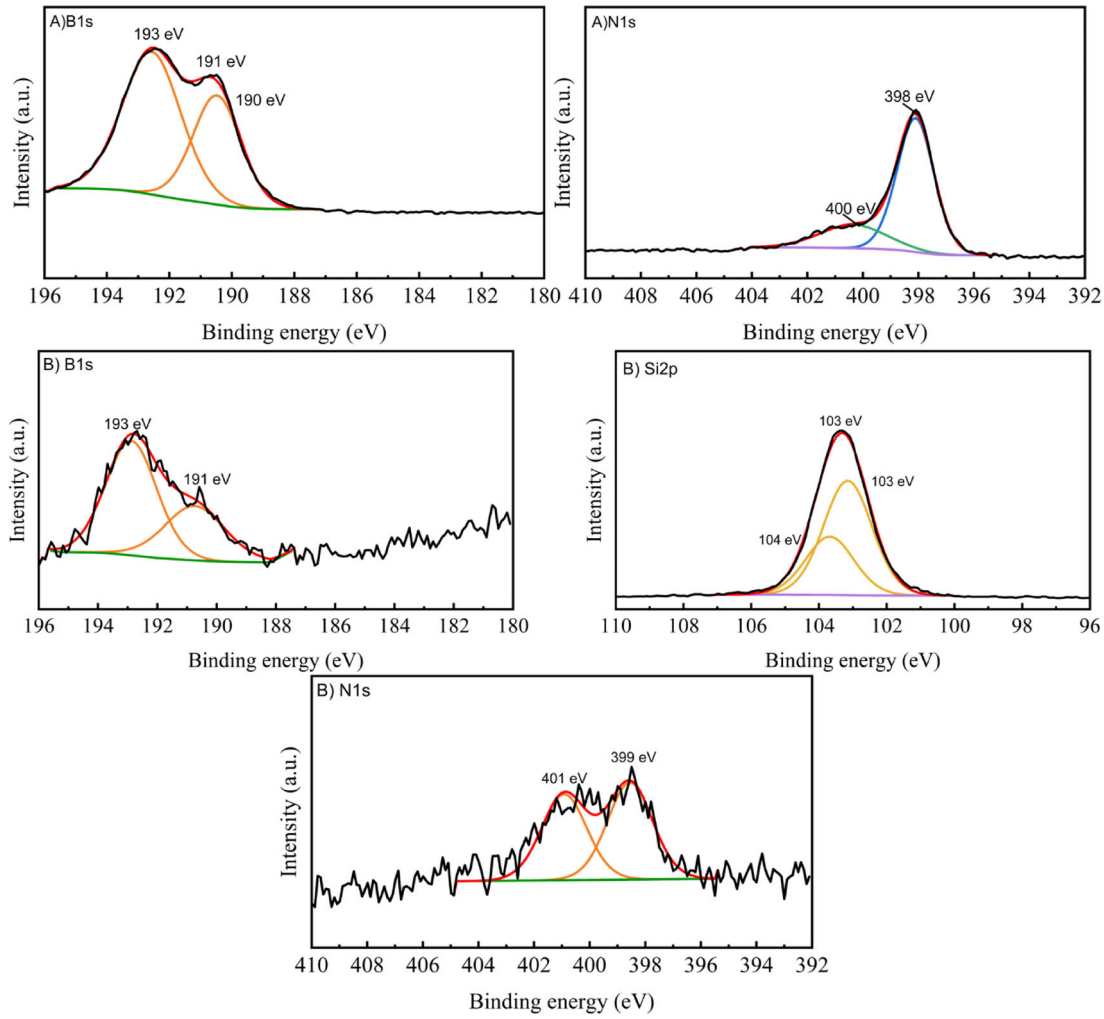


FIGURE 8 | XPS analyses of boron nitride–coated carbon fibers: (A) methyl-substituted boron nitride coated carbon fiber and (B) silicon-substituted boron nitride–coated carbon fiber.

electronic structures differ depending on the substituent type. The methyl-derived BN displays sharper and lower energy B–N and N–B peaks, characteristic of a relatively pure BN domain. Conversely, the silicon-containing sample shows broader and slightly higher-energy signals due to electronic interactions between Si–N and B–N bonds. The presence of Si–O–B linkages and surface SiO phases implies that silicon promotes oxygen retention, network crosslinking, and possibly improved coating adhesion to the carbon fiber substrate. Hence, the evolution of the B1s binding energies from 190 eV in methyl-BN to 191 eV in Si-BN—and the emergence of distinct Si2p features around 103–104 eV collectively confirms the formation of a hybrid Si–B–N ceramic coating.

Carbon fiber surfaces covered with coating can be observed via SEM analysis. Figure 9 shows that the morphology of the bare

23656549, 2025, 47, Downloaded from https://chemistry-europe.onlinelibrary.wiley.com/doi/10.1002/slct.202506905 by Yildiz Teknik Universitesi, Wiley Online Library on [16/12/2025]. See the Terms and Conditions (https://onlinelibrary.wiley.com/terms-and-conditions) on Wiley Online Library for rules of use; OA articles are governed by the applicable Creative Commons License

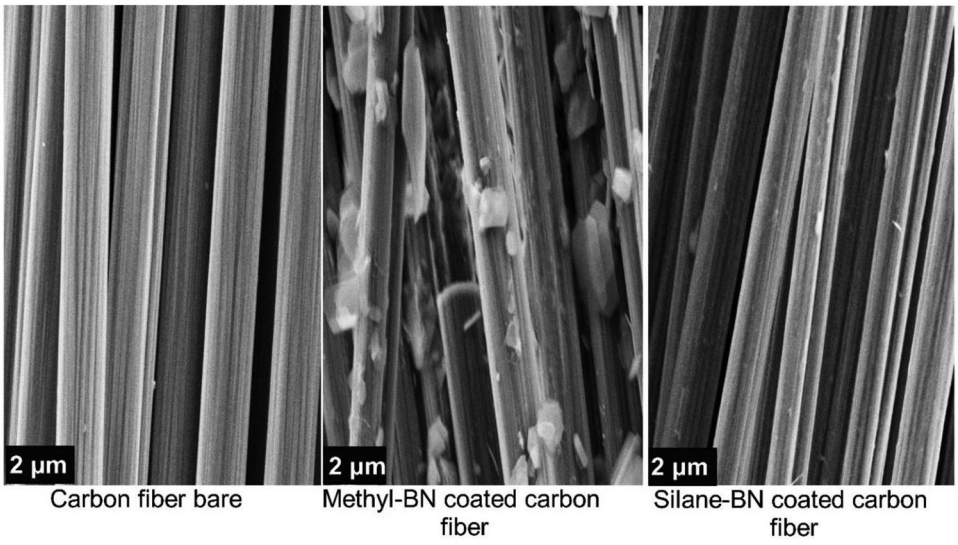


FIGURE 9 | SEM images for coated carbon fibers.

fiber changes into flakes after coating them with boron nitride. In methyl-substituted boron nitride, these flakes are more apparent and larger. In silicon-based boron nitride coating, flakes are smaller, and more uniform coating was observed. This may be because the methyl-amino borane polymer is better dispersed on the carbon fiber surface and present at a higher ratio. TGA analysis, as shown in Figure 10), also supports observed results.

An EDX analysis showed the presence of C, N, and O in the structure of methyl-based boron nitride and silicon-boron nitride. In the EDX analysis, a sharp nitrogen peak was observed due to the formation boron nitride compared to bare carbon fiber (see Figure S23). Boron cannot be detected due to presence of a sharp carbon peak. In EDX, an electron beam is focused on the material's surface to a depth of about 1 µm, whereas in XPS, the signal is acquired from a depth of only a few nm. These two methodologies' "depth of analysis" might result in a variation in the quantity [54].

The TGA analysis was also performed to investigate the thermal behavior and coating efficiencies of the fiber. Bare carbon fiber is mostly consumed at 1000°C (7.4% char yield under nitrogen). Surface coated with methyl-based polyaminoborane (turning to methyl-BN after pyrolysis) resulted in more durable (22.5% char yield) under the same condition. Si-BN coating left twice as much char residue compared to bare carbon fiber (16.2% char yield) under the same condition. In TGA, it is not uncommon to observe a percentage of residual weight greater than 100% as shown in Figure 10. Therefore, TGA analysis is repeated again, but the result persists. Nevertheless, there are some possible reasons for this uncommon result. One possible explanation is that even under N_2 conditions, trace amounts of O_2 can oxidize the surfaces and coatings. The silane-based boron nitride coating exhibited a much greater mass gain than the methyl-based boron nitride coating, likely because each Si atom contributes significantly to mass increase through the formation of SiO_2. The B–N coating also showed mass gain due to the formation of a glassy B_2O_3 layer after oxygen uptake. The bare carbon nitride sample displayed a small mass increase up to 600°C, primarily due to the presence of residual catalysts or sizing agents (e.g., metal salts, P- or Si-based sizings), which can transform into heavier inorganic phases such as oxides, phosphates, or silicates upon heating, leading to apparent mass increases and higher residual content Figure 10.

In order to determine mechanical properties, carbon fibers' maximum strain that a material can endure before breaking when stretched or pulled is measured. Automatic single-fiber test system FAVIMAT+ is used for pull-out tests for this analysis. However, BN-coated fiber was brittle for performing this test.

3 | Conclusion

Functional polyaminoboranes bearing methyl, phosphorus, and silicon groups were successfully synthesized and comprehensively characterized by NMR, GPC, TGA, and FT-IR analyses. Thermal analyses revealed that all homopolymers exhibited significant char yields above 40% at 800°C. Among them, silicon-based polyaminoboranes showed the highest char yield (60%) under a nitrogen atmosphere, whereas methyl-substituted

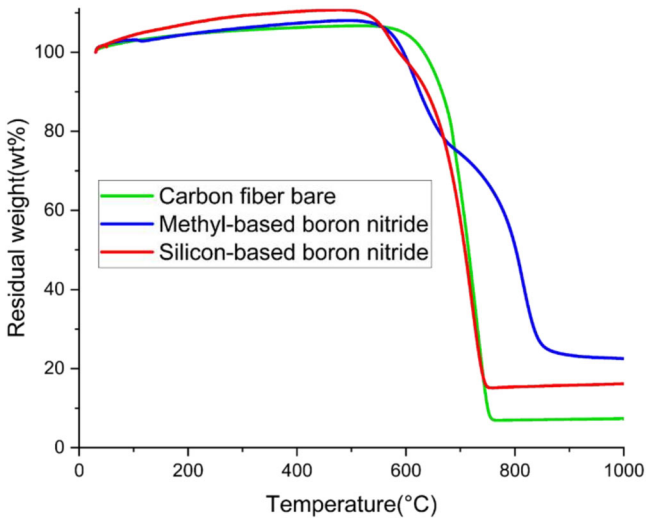


FIGURE 10 | TGA analysis of boron nitride–coated carbon fibers.

23656549, 2025, 47, Downloaded from https://chemistry-europe.onlinelibrary.wiley.com/doi/10.1002/slct.202506905 by Yildiz Teknik University, Wiley Online Library on [16/12/2025]. See the Terms and Conditions (https://onlinelibrary.wiley.com/terms-and-conditions) on Wiley Online Library for rules of use; OA articles are governed by the applicable Creative Commons License

polyaminoboranes demonstrated the best performance under air (58%). Boron nitride (BN) ceramics were obtained via pyrolysis of these polyaminoborane precursors at 1100°C for 2 h. The formation of BN was confirmed by XPS, XRD, and SEM–EDX analyses. Furthermore, carbon fiber surfaces were successfully coated with BN through the pyrolysis of functional polyaminoboranes. TGA results indicated that BN coatings derived from silicon- and methyl-based polyaminoboranes enhanced the thermal stability of carbon fibers, achieving char yields of 16% and 22%, respectively, compared to 7.4% for uncoated fibers. These findings demonstrate that functional polyaminoboranes are effective precursors for boron nitride ceramics and coatings, offering improved thermal resistance and surface protection, particularly for high-temperature composite applications.

4 | Experimental Section

4.1 | General Procedures and Equipment

Reactions were performed under nitrogen using dry solvents. For FT-IR spectroscopy (Perkin-Elmer, FT-IR), a Q50 thermal analyzer (TA Instruments, USA) was used to investigate the thermal degradation properties of polymers under nitrogen and air. NMR analysis was recorded on a Bruker AVANCE-500 NMR spectrometer operated in Fourier transform mode. Deutoro solvent d_6-DMSO and $CDCl_3$ were used as the NMR solvent. Nuclear magnetic resonance spectra were obtained using ^{1}H NMR (500 MHz), ^{11}B NMR (128 MHz), ^{13}C NMR (75 MHz), ^{31}P NMR (160 MHz), ^{29}Si NMR(80 MHz). Pyrolysis was carried out using an atmosphere-controlled tube furnace (Protherm Furnaces STF series) apparatus (Max heat capacity 1200°C) under nitrogen at 3 L min^{-1}. Surface morphology of polymers was investigated using (SEM, EVO MA15, Zeuss, Germany) coupled with (EDX, Oxford INCA 350). XPS was carried out on a Thermo Scientific *K*-Alpha spectrometer using Al *Kα* radiation to analyze the polymer powders. Crystalline form of boron nitride was determined by XRD Cu x-ray–sourced Panalytical X'Pert Pro diffractometer (Malvern Panalytical Ltd, Malvern, UK). Molecular weights and polydispersity index (*Đ*) of polymers were measured by GPC using mobile phase DMF (8% LiCl w/v) relative to polystyrene standards. For MCC, the sample chamber is heated by the controlled heating program (1 K s^{-1}) under the inert atmosphere and pyrolysis occurs. Volatiles released after pyrolysis combines with oxygen at 900°C in an oxygenated combustion calorimeter. The data obtained in this contact are used to calculate the burning temperature of pyrolysis products. Oxygen consumption and mass flow rate are converted to specific heat release (W g^{-1}) as a function of temperature. The MCC test was performed on the basis of ASTM D 7309 Method A standard.

4.2 | Reagents

All reagents were obtained from commercial sources and used without further purification unless stated otherwise. MMAB (monomethylamine–borane) (purity by titration: 97%) was purchased from Boron Specialties LLC. Ethylenediamine, diethyl chlorophosphate, triethylamine, 3-aminopropyltrimethoxysilane, borane–tetrahydrofuran complex (1.0 Molar in THF), acetonitrile, hexane, sodium hydroxide, deuterium chloroform, dichloromethane, tetrahydrofuran, and other solvents were purchased from Aldrich. Dichloro[1,3--bis(2,4,6-trimethylphenyl)-2-imidazolidinylidene] (benzylidene) (tricyclohexylphosphine)ruthenium(II) was purchased from Aldrich and used as a catalyst. For coating carbon fiber, 30K PAN-based CFFs (179 g cm^{-3}) were donated from DowAksa, Turkiye.

4.3 | Synthesis of Diethyl (2-Aminoethyl)Phosphoramidate

A 90 mL of dichloromethane was mixed with 15 mL of ethylene diamine and 1.8 mL of triethylamine. A mixture of 6 mL of dichloromethane and 1.8 mL of diethyl chlorophosphate were added dropwise over the course of 30 min to an ice bath. The reaction mixture was stirred for 3 days. Filtration was done with filter paper, and 30 mL of dichloromethane was added to the separate the fraction. The work-up was done using 3 × 30 mL 5% NaOH and 2 × 25 mL distilled water. Organic phase was filtrated after addition of drying agent $MgSO_4$ and evaporated under vacuum. Yellow precipitate was obtained and successively washed with cold diethyl ether solution to get white precipitate.

4.4 | Synthesis of Phosphorus-Based Amino Borane Monomer

Phosphorous-boron-based monomer was prepared by adding 0.2 g of diethyl (2-aminoethyl)phosphoramidate compound synthesized above and 2.5 mL of BH_3:THF complex in THF at −30°C dropwise in a dry ice-acetonitrile bath under nitrogen overnight. Then, the solvent evaporated, and white precipitate was obtained and dried. The yield was found to be 25%.

4.5 | Synthesis of Silicon-Based Amino Borane Monomer

For silicon-based precursor, 1 g of 3-aminopropyltrimethoxysilane was dissolved in THF and 5 mL of BH_3:THF complex was added dropwise to acetonitrile-dry ice bath at −30°C then mixed at room temperature for overnight. The solvent part was evaporated in a rotary-evaporator. After this step, the monomer was washed with 2–3 mL of diethyl ether and excessive pentane to mixture for purification, and this mixture waited for 1 day at −18°C. When the solvent used for washing was removed, white precipitate was obtained. The product was dried in vacuum. The yield was 33%.

4.6 | Synthesis of Methyl Functional Polyaminoboranes

Overall, 0.45 g of methylaminoborane was stirred in 0.6 mL of THF under nitrogen and then cooled to 0°C. In a separate vial, 0.045 g of dichloro[1,3-bis(2,4,6-trimethylphenyl)-2 imidazolidinylidene](benzylidene)(tricyclohexylphosphine)ruthenium(II) catalyst was dissolved in 0.4 mL of THF and added to the methylaminoborane solution. After the reaction was stirred at 0°C for 20 min under argon atmosphere, it

23656549, 2025, 47, Downloaded from https://chemistry-europe.onlinelibrary.wiley.com/doi/10.1002/slct.202506905 by Yildiz Teknik University, Wiley Online Library on [16/12/2025]. See the Terms and Conditions (https://onlinelibrary.wiley.com/terms-and-conditions) on Wiley Online Library for rules of use; OA articles are governed by the applicable Creative Commons License

was brought to room temperature and stirred at this temperature for 2 h. After adding 2–3 mL of THF to the reaction vessel at the end of the reaction, it was precipitated in excessive cold hexane–liquid nitrogen at −78°C by adding mixture in reaction vessel to this cold hexane–liquid nitrogen mixture dropwise, filtered and then dried in vacuum. Overall, 0.170 g (38% yield) of polymer in powder form was obtained.

4.7 | Synthesis of Phosphorus-Functional Polyaminoboranes

The phosphorus amine–borane precursor was mixed with the catalyst dichloro1,3-bis(2,4,6-trimethylphenyl)-2-imidazolidinylidene(tricyclohexylphosphine)ruthenium(II), which was dissolved in THF to obtain a 10 molar solution, under an argon atmosphere at room temperature. First, temperature was dropped to 0°C with ice for half hour and mixed for 2.5 h. Temperature was dropped to −78°C with liquid nitrogen and used excess hexane to precipitate out polymer. After the filtration, brown powder residue was dried under vacuum. Hexane was also used for rinsing polymers to purify them.

4.8 | Synthesis of Silicon-Functional Polyaminoboranes

In the presence of N_2 gas and at room temperature, the precursor molecule of the silicon amine–borane was mixed with the catalyst dichloro1,3-bis(2,4,6-trimethylphenyl)-2-imidazolidinylidene (tricyclohexylphosphine)ruthenium(II), which was dissolved in THF to obtain a 10-M solution. First, ice bath was used to lower the temperature to 0°C for 30 min before waiting 2.5 h to mix the reactants. Liquid nitrogen and excessive hexane were utilized to lower the temperature to −78°C, and the polymer was precipitated out from this excessive hexane solution. Brown powder leftovers were vacuum-dried after filtering.

4.9 | Synthesis of Boron Nitride From Functionalized Polyaminoboranes

Polyaminoboranes are used as precursors for synthesis of boron nitride–based ceramic materials. Pyrolysis was carried out using an atmosphere-controlled tube furnace (Protherm Furnaces STF series) apparatus (Max heat capacity 1200°C) under nitrogen at 2 L min^{-1}. Methyl, silicon, and phosphorus polyaminoboranes were pyrolyzed at 1100°C under nitrogen for 2 h.

4.10 | Carbon Fiber Coating Application

Overall, 10 cm carbon fiber filaments were immersed in 10% coating solutions obtained by dissolving the synthesized functional polyaminoboranes in THF. Samples immersed for 30 min were dried under a fume hood for 1 h. After that, pyrolysis was conducted at 1100°C under nitrogen for 2 h.

Acknowledgments

This work was supported by the project no "FBA-2022-4124 Synthesis and applications of functional polyaminoboranes (carbon fiber used in aircraft and coating the surface of aluminum parts and using as a flame retardant in paint varnish formulation)" of YTU Coordinatorship of Scientific Research Projects. Support from EU COST Action CM1302 "Smart Inorganic Polymers (SIPs)" is also gratefully acknowledged.

Conflicts of Interest

The authors declare no conflicts of interest.

Data Availability Statement

The data that support the findings of this study are available in the Supporting Information section of this article.

References

1. W. Kaminsky, "Trends in Polyolefin Chemistry," *Macromolecular Chemistry and Physics* 209 (2008): 459–466, https://doi.org/10.1002/macp.200700575.

2. A. Staubitz, M. E. Sloan, A. P. M. Robertson, et al., "Catalytic Dehydrocoupling/Dehydrogenation of N-Methylamine-Borane and Ammonia-Borane: Synthesis and Characterization of High Molecular Weight Polyaminoboranes," *Journal of the American Chemical Society* 132 (2010): 13332–13345, https://doi.org/10.1021/ja104607y.

3. J. Green, "A Review of Phosphorus-Containing Flame Retardants," *Journal of Fire Sciences* 10 (1992): 470–487, https://doi.org/10.1177/073490419201000602.

4. H. Dorn, R. A. Singh, J. A. Massey, et al., "Transition Metal-Catalyzed Formation of Phosphorus−Boron Bonds: A New Route to Phosphinoborane Rings, Chains, and Macromolecules," *Journal of the American Chemical Society* 122 (2000): 6669–6678, https://doi.org/10.1021/ja000732r.

5. C. A. Jaska, K. Temple, A. J. Lough, and I. Manners, "Transition Metal-Catalyzed Formation of Boron−Nitrogen Bonds: Catalytic Dehydrocoupling of Amine-Borane Adducts to Form Aminoboranes and Borazines," *Journal of the American Chemical Society* 125 (2003): 9424–9434, https://doi.org/10.1021/ja0301601.

6. M. C. Denney, V. Pons, T. J. Hebden, D. M. Heinekey, and K. I. Goldberg, "Efficient Catalysis of Ammonia Borane Dehydrogenation," *Journal of the American Chemical Society* 128 (2006): 12048–12049, https://doi.org/10.1021/ja062419g.

7. A. Staubitz, A. Presa Soto, and I. Manners, "Iridium-Catalyzed Dehydrocoupling of Primary Amine–Borane Adducts: A Route to High Molecular Weight Polyaminoboranes, Boron–Nitrogen Analogues of Polyolefins," *Angewandte Chemie International Edition* 47 (2008): 6212–6215, https://doi.org/10.1002/anie.200801197.

8. S. Bhunya, T. Malakar, and A. Paul, "Unfolding the Crucial Role of a Nucleophile in Ziegler–Natta Type Ir Catalyzed Polyaminoborane Formation," *Chemical Communications* 50 (2014): 5919–5922, https://doi.org/10.1039/c4cc01337a.

9. G. I. Peterson and T.-L. Choi, "Cascade Polymerizations: Recent Developments in the Formation of Polymer Repeat Units By Cascade Reactions," *Chemical Science* 11 (2020): 4843–4854, https://doi.org/10.1039/D0SC01475C.

10. L. Alig, M. Fritz, and S. Schneider, "First-Row Transition Metal (De)Hydrogenation Catalysis Based on Functional Pincer Ligands," *Chemical Reviews* 119 (2019): 2681–2751, https://doi.org/10.1021/acs.chemrev.8b00555.

11. C. N. Brodie, T. M. Boyd, L. Sotorríos, et al., "Controlled Synthesis of Well-Defined Polyaminoboranes on Scale Using a Robust and Efficient Catalyst," *Journal of the American Chemical Society* 143 (2021): 21010–21023, https://doi.org/10.1021/jacs.1c10888.

12. S. Pandey, P. Lönnecke, and E. Hey-Hawkins, "Phosphorus–Boron-Based Polymers Obtained By Dehydrocoupling of Ferrocenylphosphine–Borane Adducts," *European Journal of Inorganic Chemistry* 2014 (2014): 2456–2465, https://doi.org/10.1002/ejic.201402021.

23656549, 2025, 47, Downloaded from https://chemistry-europe.onlinelibrary.wiley.com/doi/10.1002/slct.202506905 by Yildiz Teknik University, Wiley Online Library on [16/12/2025]. See the Terms and Conditions (https://onlinelibrary.wiley.com/terms-and-conditions) on Wiley Online Library for rules of use; OA articles are governed by the applicable Creative Commons License

13. G. Alcaraz, L. Vendier, E. Clot, and S. Sabo-Etienne, "Ruthenium Bis(σ-B–H) Aminoborane Complexes From Dehydrogenation of Amine–Boranes: Trapping of H_2B–NH_2," *Angewandte Chemie International Edition* 49 (2010): 918–920, https://doi.org/10.1002/anie.200905970.

14. A. L. Colebatch, B. W. Hawkey Gilder, G. R. Whittell, N. L. Oldroyd, I. Manners, and A. S. Weller, "A General, Rhodium-Catalyzed, Synthesis of Deuterated Boranes and N-Methyl Polyaminoboranes," *Chemistry—A European Journal* 24 (2018): 5450–5455, https://doi.org/10.1002/chem.201800737.

15. P. Paetzold, "Iminoboranes," *Advances in Inorganic Chemistry* 31 (1987): 123–170, https://doi.org/10.1016/S0898-8838(08)60223-8.

16. R. B. Kaner, J. J. Gilman, and S. H. Tolbert, "Materials Science. Designing Superhard Materials," *Science* 2005 (1979): 1268–1269.

17. J. J. Pouch and S. A. Alterovitz, "A Review of: "Synthesis and Properties of Boron Nitride"," *Materials and Manufacturing Processes* 6 (1991): 373–374, https://doi.org/10.1080/10426919108934766.

18. R. Naslain, A. Guette, F. Rebillat, R. Pailler, F. Langlais, and X. Bourrat, "Boron-Bearing Species in Ceramic Matrix Composites for Long-Term Aerospace Applications," *Journal of Solid State Chemistry* 177 (2004): 449–456, https://doi.org/10.1016/j.jssc.2003.03.005.

19. R. K. Kountanya and P. Boppana, "Optimization of Machining of Automotive Components With Polycrystalline Cubic Boron Nitride," *Proceedings of the Institution of Mechanical Engineers, Part B: Journal of Engineering Manufacture* 222 (2008): 797–805, https://doi.org/10.1243/09544054JEM1043.

20. J. Bao, K. Jeppson, M. Edwards, et al., "Synthesis and Applications of Two-Dimensional Hexagonal Boron Nitride in Electronics Manufacturing," *Electronic Materials Letters* 12 (2016): 1–16, https://doi.org/10.1007/s13391-015-5308-2.

21. C. Zhou, C. Lai, C. Zhang, et al., "Semiconductor/Boron Nitride Composites: Synthesis, Properties, and Photocatalysis Applications," *Applied Catalysis B: Environmental* 238 (2018): 6–18, https://doi.org/10.1016/j.apcatb.2018.07.011.

22. G. Cassabois, P. Valvin, and B. Gil, "Hexagonal Boron Nitride Is an Indirect Bandgap Semiconductor," *Nature Photonics* 10 (2016): 262–266, https://doi.org/10.1038/nphoton.2015.277.

23. L. M. S. Ansaloni and E. M. B. de Sousa, "Boron Nitride Nanostructured: Synthesis, Characterization and Potential Use in Cosmetics," *Materials Sciences and Applications* 04 (2013): 22–28, https://doi.org/10.4236/msa.2013.41004.

24. A. Lipp, K. A. Schwetz, and K. Hunold, "Hexagonal Boron Nitride: Fabrication, Properties and Applications," *Journal of the European Ceramic Society* 5 (1989): 3–9, https://doi.org/10.1016/0955-2219(89)90003-4.

25. R. T. Paine and C. K. Narula, "Synthetic Routes to Boron Nitride," *Chemical Reviews* 90 (1990): 73–91, https://doi.org/10.1021/cr00099a004.

26. S. Ogawa, S. Fukushima, and M. Shimatani, "Hexagonal Boron Nitride for Photonic Device Applications: A Review," *Materials* 16 (2023): 2005.

27. T. Wideman, P. J. Fazen, K. Su, E. E. Remsen, G. A. Zank, and L. G. Sneddon, "Second-Generation Polymeric Precursors for BN and SiNCB Ceramic Materials," *Applied Organometallic Chemistry* 12 (1998): 681–693, https://doi.org/10.1002/(SICI)1099-0739(199810/11)12:10/11%3c681::AID-AOC786%3e3.0.CO;2-D.

28. S.-K. Kim, H. Cho, M. J. Kim, et al., "Efficient Catalytic Conversion of Ammonia Borane to Borazine and Its Use for Hexagonal Boron Nitride (White Graphene)," *Journal of Materials Chemistry A* 1 (2013): 1976–1981, https://doi.org/10.1039/C2TA00758D.

29. V. A. Du, T. Jurca, G. R. Whittell, and I. Manners, "Aluminum Borate Nanowires From the Pyrolysis of Polyaminoborane Precursors," *Dalton Transactions* 45 (2016): 1055–1062, https://doi.org/10.1039/C5DT03324A.

30. D.-P. Kim, K.-T. Moon, J.-G. Kho, J. Economy, C. Gervais, and F. Babonneau, "Synthesis and Characterization of Poly(Aminoborane) as a New Boron Nitride Precursor," *Polymers for Advanced Technologies* 10 (1999): 702–712, https://doi.org/10.1002/(SICI)1099-1581(199912)10:12%3c702::AID-PAT931%3e3.0.CO;2-Q.

31. L. G. Sneddon, M. G. L. Mirabelli, A. T. Lynch, P. J. Fazen, K. Su, and J. S. Beck, "Polymeric Precursors to Boron Based Ceramics," *Pure and Applied Chemistry* 63 (1991): 407–410, https://doi.org/10.1351/pac199163030407.

32. S. Bernard and P. Miele, "Nanostructured and Architectured Boron Nitride From Boron, Nitrogen and Hydrogen-Containing Molecular and Polymeric Precursors," *Materials Today* 17 (2014): 443–450, https://doi.org/10.1016/j.mattod.2014.07.006.

33. Z. Cheng, W. Xu, D. Ding, C. Xu, Y. Xie, and M. Qiao, "Preparation of Boron Nitride Hybrid Containing Phosphorus and Silicon and Its Effect on Flame Retardant, Smoke Suppression, and Thermal Conductivity Properties of Styrene-Butadiene Rubber," *Journal of Applied Polymer Science* 139 (2022): e53071, https://doi.org/10.1002/app.53071.

34. H. Huang, H. Wang, Y. Xie, D. Dong, X. Jiang, and X. Zhang, "Incorporation of Boron Nitride Nanosheets in Zinc Phosphate Coatings on Mild Steel to Enhance Corrosion Resistance," *Surface and Coatings Technology* 374 (2019): 935–943, https://doi.org/10.1016/j.surfcoat.2019.06.082.

35. J. Sun, Z. Tang, G. Meng, and L. Gu, "Silane Functionalized Plasma-Treated Boron Nitride Nanosheets for Anticorrosive Reinforcement of Waterborne Epoxy Coatings," *Progress in Organic Coatings* 167 (2022): 106831, https://doi.org/10.1016/j.porgcoat.2022.106831.

36. K. C. Yung and H. Liem, "Enhanced Thermal Conductivity of Boron Nitride Epoxy-Matrix Composite Through Multi-Modal Particle Size Mixing," *Journal of Applied Polymer Science* 106 (2007): 3587–3591, https://doi.org/10.1002/app.27027.

37. A.-F. Shao, Z.-B. Wang, Y.-Y. Chu, Z.-Z. Jiang, G.-P. Yin, and Y. Liu, "Evaluation of the Performance of Carbon Supported Pt–Ru–Ni–P as Anode Catalyst for Methanol Electrooxidation," *Fuel Cells* 10 (2010): 472–477, https://doi.org/10.1002/fuce.200900170.

38. A. R. J. Kucernak, K. F. Fahy, and V. N. N. Sundaram, "Facile Synthesis of Palladium Phosphide Electrocatalysts and Their Activity for the Hydrogen Oxidation, Hydrogen Evolutions, Oxygen Reduction and Formic Acid Oxidation Reactions," *Catalysis Today* 262 (2016): 48–56, https://doi.org/10.1016/j.cattod.2015.09.031.

39. S. Iliescu, E. Avram, A. Visa, N. Plesu, A. Popa, and G. Ilia, "New Technique for the Synthesis of Polyphosphoesters," *Macromolecular Research* 19 (2011): 1186–1191, https://doi.org/10.1007/s13233-011-11-11-6.

40. P. Sannigrahi and E. Ingall, "Polyphosphates as a Source of Enhanced P Fluxes in Marine Sediments Overlain By Anoxic Waters: Evidence From ^{31}P NMR," *Geochemical Transactions* 6 (2005): 52, https://doi.org/10.1186/1467-4866-6-52.

41. F. Anke, S. Boye, A. Spannenberg, A. Lederer, D. Heller, and T. Beweries, "Dehydropolymerisation of Methylamine Borane and an N-Substituted Primary Amine Borane Using a PNP Fe Catalyst," *Chemistry—A European Journal* 26 (2020): 7889–7899, https://doi.org/10.1002/chem.202000809.

42. M. L. Nielsen, J. V. Pustinger, and J. Strobel, "Phosphorus-31 Nuclear Magnetic Resonance Chemical Shifts of Phosphorus Compounds," *Journal of Chemical & Engineering Data* 9 (1964): 167–170, https://doi.org/10.1021/je60021a003.

43. E. Herth, R. Zeggari, J.-Y. Rauch, F. Remy-Martin, and W. Boireau, "Investigation of Amorphous SiOx Layer on Gold Surface for Surface Plasmon Resonance Measurements," *Microelectronic Engineering* 163 (2016): 43–48, https://doi.org/10.1016/j.mee.2016.04.014.

44. J. Qu, Q. Li, C. Luo, J. Cheng, and X. Hou, "Characterization of Flake Boron Nitride Prepared From the Low Temperature Combustion Synthesized Precursor and Its Application for Dye Adsorption," *Coatings* 8 (2018): 214, https://doi.org/10.3390/coatings8060214.

45. M. Kanat and T. Eren, "Synthesis of Phosphorus-Containing Flame Retardants and Investigation of Their Flame Retardant Behavior in

23656549, 2025, 47, Downloaded from https://chemistry-europe.onlinelibrary.wiley.com/doi/10.1002/slct.202506905 by Yildiz Teknik University, Wiley Online Library on [16/12/2025]. See the Terms and Conditions (https://onlinelibrary.wiley.com/terms-and-conditions) on Wiley Online Library for rules of use; OA articles are governed by the applicable Creative Commons License

Textile Applications," *Journal of Applied Polymer Science* 136 (2019): 47935, https://doi.org/10.1002/app.47935.

46. H. Harrison, J. T. Lamb, K. S. Nowlin, et al., "Quantification of Hexagonal Boron Nitride Impurities in Boron Nitride Nanotubes Via FTIR Spectroscopy," *Nanoscale Advances* 1 (2019): 1693–1701, https://doi.org/10.1039/C8NA00251G.

47. N. Kostoglou, K. Polychronopoulou, and C. Rebholz, "Thermal and Chemical Stability of Hexagonal Boron Nitride (h-BN) Nanoplatelets," *Vacuum* 112 (2015): 42–45, https://doi.org/10.1016/j.vacuum.2014.11.009.

48. M. Li, M. Wang, X. Hou, et al., "Highly Thermal Conductive and Electrical Insulating Polymer Composites With Boron Nitride," *Composites Part B: Engineering* 184 (2020): 107746, https://doi.org/10.1016/j.compositesb.2020.107746.

49. L. H. Li, J. Cervenka, K. Watanabe, T. Taniguchi, and Y. Chen, "Strong Oxidation Resistance of Atomically Thin Boron Nitride Nanosheets," *ACS Nano* 8 (2014): 1457–1462, https://doi.org/10.1021/nn500059s.

50. Y. Kimura, T. Wakabayashi, K. Okada, T. Wada, and H. Nishikawa, "Boron Nitride as a Lubricant Additive," *Wear* 232 (1999): 199–206, https://doi.org/10.1016/S0043-1648(99)00146-5.

51. Y. Uchida, K. Kawahara, S. Fukamachi, and H. Ago, "Chemical Vapor Deposition Growth of Uniform Multilayer Hexagonal Boron Nitride Driven By Structural Transformation of a Metal Thin Film," *ACS Applied Electronic Materials* 2 (2020): 3270–3278, https://doi.org/10.1021/acsaelm.0c00601.

52. M. Djouadi, "Deposition of Boron Nitride Films By PVD Methods: Transition From h-BN to c-BN," *Surface and Coatings Technology* 180–181 (2004): 174–177, https://doi.org/10.1016/j.surfcoat.2003.10.156.

53. X. Huang, "Fabrication and Properties of Carbon Fibers," *Materials* 2 (2009): 2369–2403, https://doi.org/10.3390/ma2042369.

54. I. C. Çetinkaya, G. Yüksel, C. Macit, M. E. Üreyen, and T. Eren, "Synthesis and Characterization of Polyphosphonates and Polyurethanes Using Chalcone and DOPO-Chalcone as a Flame Retardant," *ACS Applied Polymer Materials* 3 (2021): 5277–5290, https://doi.org/10.1021/acsapm.1c01054.

Supporting Information

Additional supporting information can be found online in the Supporting Information section.

Supporting File: slct72106-sup-0001-SuppMat.docx Figure S5 and Figure S9 are revised.

23656549, 2025, 47, Downloaded from https://chemistry-europe.onlinelibrary.wiley.com/doi/10.1002/slct.202506905 by Yildiz Teknik University, Wiley Online Library on [16/12/2025]. See the Terms and Conditions (https://onlinelibrary.wiley.com/terms-and-conditions) on Wiley Online Library for rules of use; OA articles are governed by the applicable Creative Commons License